Biological super-resolution imaging by using novel microsphere-embedded coverslips

Arash Darafsheh[*a], Consuelo Guardiola[a], Deepak Nihalani[b], Daeyeon Lee[c], Jarod C. Finlay[a], and Alejandro Cárabe[a]

[a]Department of Radiation Oncology, University of Pennsylvania, Philadelphia, PA 19104, USA;
[b]Renal-Electrolyte and Hypertension Division, University of Pennsylvania, Philadelphia, PA 19104, USA;
[c]Department of Chemical and Biomolecular Engineering, University of Pennsylvania, Philadelphia, PA 19104, USA

ABSTRACT

Optical super-resolution imaging is a desirable technique in many fields, including medical and material sciences and nanophotonics. We demonstrated feasibility of optical microscopy, with resolution improvement by a factor of 2-3, by using microsphere-embedded coverslips composed of barium titanate glass microspheres (refractive index n~1.9-2.1) fixed in a transparent layer of polydimethylsiloxane. Imaging was performed by a conventional microscope and a fluorescent microscope with the microsphere-embedded layer placed in a contact position with various biological specimens and semiconductor nanostructures. We investigated a biomedical application of microsphere-assisted imaging technique by immunostaining of kidney sections where cellular distribution of a motor protein Myo1c and a podocyte specific protein ZO-1 was analyzed. A significant visual enhancement in the distribution pattern of the proteins was noted in the stained glomeruli by using microsphere-assisted imaging technique. Our results suggest that microsphere-assisted imaging technique is a promising candidate for applications in medical and cancer research, as well as in microfluidics and nanophotonics.

Keywords: Super-resolution, microscopy, nanoscopy, microsphere, barium titanate, PDMS, biological imaging.

1. INTRODUCTION

The far-field spatial resolution of any standard lens-based optical microscope is fundamentally limited by the wavelength of the imaging light and the numerical aperture (NA) of the objective lens system due to diffraction of light waves. NA is defined by $NA=n\times\sin\theta$, in which n is the refractive index of the object-space medium and θ is the half-angle of the maximum cone of light that can enter (exit) the lens. For conventional white-light microscope systems Abbe's diffraction-limit is $0.5\lambda/NA$~250 nm. Improving the imaging resolution significantly impacts several disciplines, such as life and material sciences and nanophotonics, and therefore has been the subject of considerable research effort.

Immersed microsphere-assisted imaging technique [1, 2] is a remarkably simple approach toward achieving high-resolution imaging. In this technique, microspheres with high index of refraction (n~2), embedded in an elastomer layer, are used as microscope coverslips to collect high spatial frequency harmonics present in the optical near-field of the object and transmit them to the far-field with magnification providing high resolution imaging. In comparison with imaging through liquid-immersed microspheres [1, 3, 4], by fixing the microspheres in elastomers such layers can be pre-fabricated and used as coverslips, imaging can be performed by an inverted microscope, and any potential influence of liquid evaporation on imaging performance is minimized.

[*]Corresponding author: arash.darafsheh@gmail.com

Nanoscale Imaging, Sensing, and Actuation for Biomedical Applications XII, edited by Alexander N. Cartwright, Dan V. Nicolau,
Proc. of SPIE Vol. 9337, 933705 · © 2015 SPIE · CCC code: 1605-7422/15/$18 · doi: 10.1117/12.2078019

In the present work we apply microsphere-assisted imaging technique for imaging various biological structures. Our results indicate potential advantages of immersed microsphere-assisted super-resolution imaging technique in developing various applications in biomedical imaging and nanophotonics.

2. IMAGING TECHNIQUE

A schematic of the experimental setup is illustrated in Fig. 1(a) in which the microsphere-embedded polydimethylsiloxane (PDMS) layer is placed over the specimen as a microscope coverslip and an upright microscope in reflection illumination mode is used for imaging. A magnified virtual image is formed by each sphere underneath the specimen's surface that is captured by the objective lens, as illustrated in Fig. 1(b). We used a commercial Blu-ray® disk (BD), the structure of which consists of parallel 200-nm-stripes separated by 100-nm-grooves, as the imaging object. In order to fabricate the microsphere-embedded films we used two modifications of barium titanate glass (BTG) microspheres (Mo-Sci Corp.) differing by their chemical composition and, as a result, by their index of refraction (n~1.9 and ~2.1). BTG microspheres with diameters D~30-150 μm were dispersed over the BD sample and a microscope cover glass as the substrates by self-assembly; then liquid PDMS elastomer (Dow Corning®) with index n_m~1.41 and proportion 1:10 of cure compound was extended over the microspheres by using spin-coating. The thickness of the film was controlled by the coating speed and spinning duration. The compound was baked at 65°C for 1 hour to dry the mixed compound and form a removable microsphere-embedded layer. We fabricated such layers with various thicknesses up to 300 μm.

The structure of the BD cannot be resolved by conventional microscopy using a 100×(0.95NA) objective lens. However, imaging of the BD structure is possible through high-index BTG microspheres embedded in the PDMS layer, as shown in Fig. 1(c) for a microsphere with D~60μm (n~1.9) through a 100×(0.9NA) objective lens. We obtained similar results through a 50×(0.45NA) objective lens. We found that the layers with higher index microspheres (n~2.1) produce higher magnification factors and larger fields-of-view. It should be noted that high-index microspheres do not form an image when the ambient medium is air, i.e. prior to immersion in elastomers. However, when they are immersed in liquids and elastomers, due to the modification of the refractive index contrast caused by the ambient medium, imaging is possible [2].

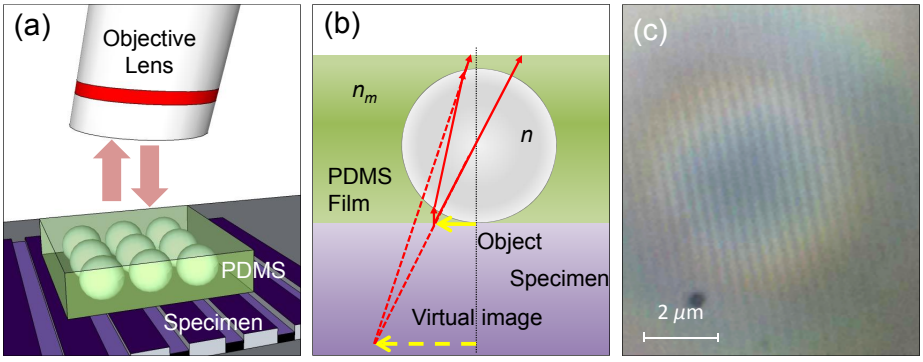

Figure 1. (a) Schematic of the experimental setup with microspheres embedded in a PDMS layer positioned over the specimen. (b) A virtual image is formed underneath the specimen's surface. (c) the structure of the Blu-ray disk is resolved through a BTG microsphere with D~60μm (n~1.9) embedded in the PDMS layer [2].

3. SPATIAL RESOLUTION

Improved resolution of microsphere-assisted imaging stems from several factors. For all sphere diameters, the resolution is improved due to enhancement of the effective NA of the system. Geometrical optics treatment gives $NA_s = n \times Sin\theta / (2-n)$, where n is the refractive index of the sphere, for the combined system of the objective lens and a sphere working in air. It should be noted that the maximum achievable NA is n in this case. However, for micron-scale spheres, the super-resolution strength can be additionally enhanced due to "photonic nanojet" properties of

microspheres [1, 5]. Focusing properties of microspheres, such as "photonic nanojets" [6] and "periodically focused modes" [1, 7, 8] have motivated their application in light focusing and imaging devices [7-12].

One important issue that we point out in this work is that in order to assess the resolution improvement introduced by using the microspheres, one must adopt an approach consistent with classic definition of "resolution". There are several classic criteria defining the spatial resolution of an imaging system; among them, Rayleigh [13] and Houston [14] criteria are used most widely. In this work, we considered Houston criterion that is more practical especially in cases where the intensity profile of the focal spot does not fall to zero due to lens aberrations or noise. According to Houston criterion, two "point sources" with equal intensities are just resolved if the distance between the central maxima of the intensity distribution in the image plane is equal to the full-width-at-half-maximum (FWHM) of the intensity distribution of either point source. In this way, the FWHM of the system's point-spread function (PSF) is practically used as the measure of the spatial resolution. Houston criterion gives $0.515\lambda/\mathrm{NA}$ as the resolution limit for a lens with circular aperture. Since the image can be seen as a convolution of the imaging system's PSF and the object [15], the PSF can be measured through deconvolution of the object and image functions.

As stated above, classic definitions of resolution are defined for "point source" objects, whereas in reality objects have finite sizes. Neglecting the effect of the size of the structures on the object and just considering the distance between them (edge-to-edge or center-to-center) as the achieved resolution leads to misleading claims of resolution. In the following, we demonstrate this point by giving a few examples and provide a robust approach in assessing the achieved spatial resolution.

In the first example, as the object function we considered two parallel bars with width w separated by a gap g, in which $2w+g$=500 nm, see Fig. 2(a). The image profile shown in Fig. 2(i) is obtained by convolving the object profile [Fig. 2(a), w=200 and g=100 nm] with the PSF presented in Fig. 2(e) (an Airy pattern with 230 nm FWHM). We found that a system with 230-nm resolution can discern the 100-nm gap in the object profile presented in Fig. 2(a). The image profile presented in Fig. 2(j) is obtained by convolving the object profile shown in Fig. 2(b) with a PSF with 100-nm FWHM [Fig. 2(f)]. Although the 100-nm gap is resolved in both cases, as the PSF becomes narrower, the ratio of peak-to-saddle intensity becomes greater indicating better spatial resolution in the latter.

Similarly, Fig. 2(k) is obtained by convolving the object profile [Fig. 2(c), w=240 and g=20 nm] with the PSF [Fig. 2(g)] with 97 nm FWHM. The calculation result presented in Fig. 2(k) demonstrates that the required spatial resolution to visualize the 20 nm gap in the object profile shown in Fig. 2(c) is ~100 nm not necessarily 20 nm. This point is very important and shows that there would be 5-fold error in assessing the spatial resolution of the system if by mere visualization of the 20-nm gap, one claims 20-nm "resolution". The image profile shown in Fig. 2(l) is obtained by convolving the object profile shown in Fig. 2(d) with a PSF with 20 nm FWHM [Fig. 2(h)] that shows for the system with 20-nm resolution, the peak-to-saddle intensity in the image is ~0.25 for that object.

These examples clearly show that in order to evaluate the spatial resolution of the imaging system, caution must be exercised when dealing with structures with finite sizes, such as the Blu-ray disk or similar structures, instead of "point sources". The convolution method, however, provides a systematic approach consistent with classic definition of resolution in order to measure the achieved spatial resolution obtained in microsphere-assisted imaging.

We varied the ratio of w/g in the object profile shown in Fig. 1(a) in the range 2-12 that corresponds to gap sizes of 100-20 nm, and calculated the required FWHM of the PSF that leads to peak-to-saddle ratio of 0.81 in the calculated image profiles in each case. The choice of 0.81 as the saddle irradiance is according to the generalized Rayleigh criterion for resolution [16]. The required resolution, defined as the FWHM of the PSF, in order to resolve each object is presented in Fig. 3 as a function of the gap size in the structure. Fig. 3 shows that there would be 2-5 times error in measuring the spatial resolution if by mere visualization of the gap g, one claims g-nm "resolution".

In [2], Darafsheh *et al*. pointed out the inconsistency in the literature in assessing resolution gain in microsphere-assisted imaging technique; and proposed the use of convolution method to measure the resolution and measured ~$\lambda/4$ resolution for BTG spheres (D>50 μm) embedded in PDMS. It should be noted that resolution ~$\lambda/6$-$\lambda/5$ is expected [1] for microspheres with smaller diameters ($5<D<10$ μm). However there is a tradeoff between resolution gain and field-of-view since the field-of-view decreases as the diameter of the sphere decreases.

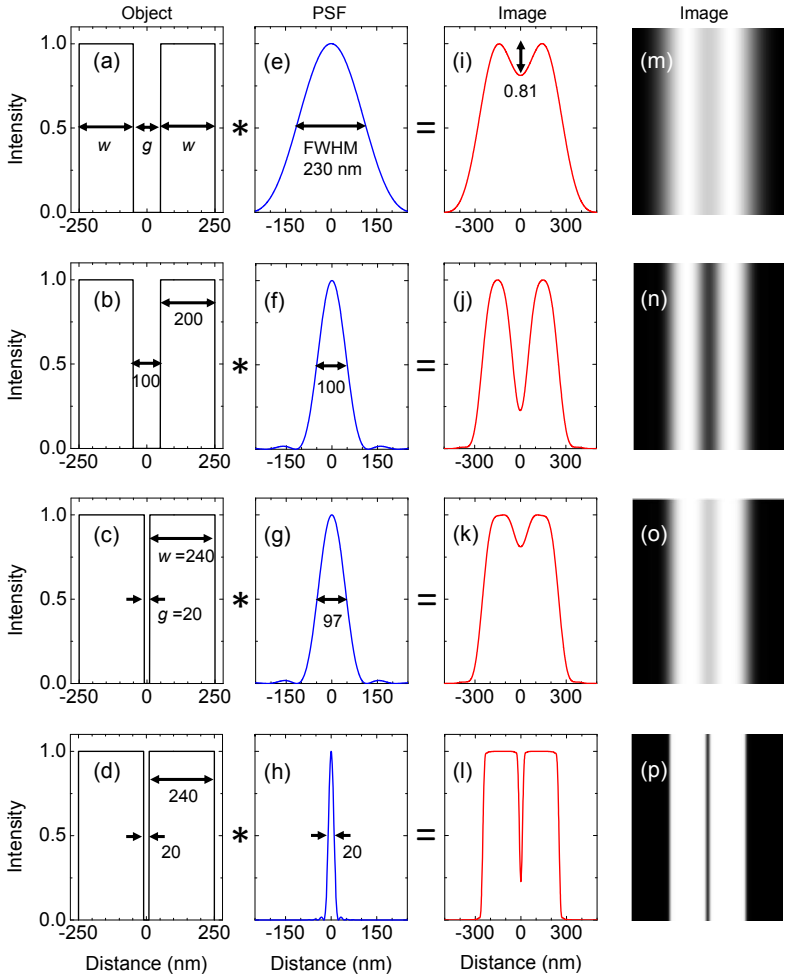

Figure 2. (a,b) and (c,d) Intensity profiles of the objects with bars with width w = 200 and 240 nm separated by a g =100 and 20 nm gap, respectively. (e-h) Point-spread functions with FWHM = 230, 100, 97, and 20 nm, respectively. (i-l) Calculated image profiles obtained from (i)=(a)∗(e), (j)=(b)∗(f), (k)=(c)∗(g), and (l)=(d)∗(h), respectively. (m-p) Image patterns corresponding to profiles shown in (i-l), respectively.

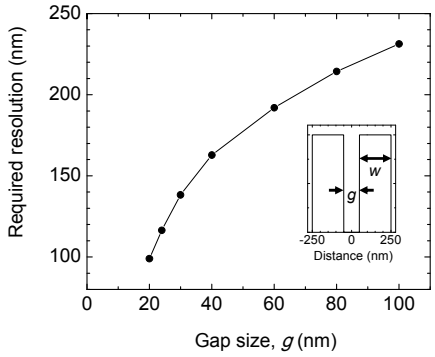

Figure 3. Required spatial resolution for resolving two stripes with width w separated by a gap g=500-2w nm, shown in the inset, as a function of the gap size, g.

4. BIOLOGICALIMAGING

In [2], the feasibility of biological imaging by using microsphere-embedded coverslips for imaging of radiation-induced γ-H2AX foci formation in U87 glioblastoma cells irradiated by ionizing radiation, such as proton beams, was demonstrated.

Here, we investigated the application of microsphere-assisted imaging for imaging mouse kidney sections. Majority of glomerular diseases [17] that affect kidney function are diagnosed through the histological analysis of kidney sections. The pathologists screen these sections for changes in the structure of the various cell types within a glomerulus, such as the glomerular basement membrane, podocytes and endothelial cells. In addition, they look for lesions and scarring in the glomeruli to study the extent of a disease. In order to understand the severity of a disease, more often high resolution imaging of the tissue sections is desired which requires additional processing of the samples and subjecting them to electron microscopy or other high resolution imaging modalities. Since microsphere-assisted imaging method can enhance the ability of a standard microscope to visualize the affected regions in the tissue by several folds, it helps in diagnosing the disease economically without subjecting the tissue to a more extensive imaging analysis.

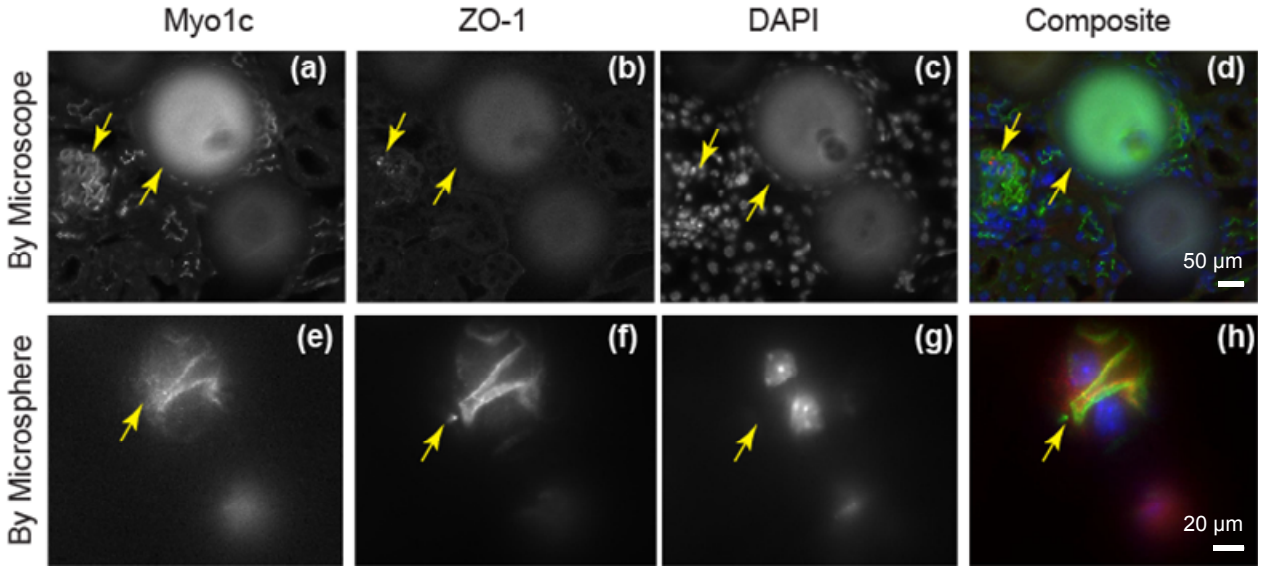

Figure 4.Top row: Fluorescent micrographs of glomeruli stained for (a) Myo1c, (b) ZO-1, and (c) DAPI (arrows), (d) composite image of (a-c). Bottom row: (e-g) glomeruli stained for Myo1c, ZO-1, and DAPI, respectively, imaged through a BTG microsphere, (h) the composite image of (e-g).

Kidney sections from mice were immunostained with antibodies against podocyte protein markers ZO-1 (Alexa 488, green) and Myo1c (Alexa 568, red). Following staining the stained sections were mounted with gold antifade mounting solution (Invitrogen) containing BTG microspheres with ~80 µm diameter and refractive index n~2.1. The stained glomeruli were visualized by epifluorescence microscopy using an Olympus 1X70 microscope through a 25×(NA=0.8) oil immersion objective. Figs.4(a-c) show fluorescent micrographs of glomeruli stained for Myo1c, ZO-1, and DAPI (arrows), respectively, imaged through the objective lens without using the microsphere and Fig. 4(d) is the composite of the three panels in the top row. Figs. 4(e-g) show the glomeruli that are imaged by focusing through the sphere on the virtual image formed by the sphere and Fig. 4(h) shows the composite of the three panels in the bottom row. All parameters were kept constant, including exposure time while taking images. Comparing the bottom panels in Fig. 4 with the top panels shows the improvements obtained by imaging through the microsphere. As shown in the top panels of Fig. 4, it is difficult to notice the colocalization of Myo1c with ZO-1. However, in the bottom panels of Fig. 4, where the images were captured through the microsphere, a clear colocalization of Myo1c with ZO-1 at the podocyte cell membrane within the glomerulus is observed. From a research perspective, microsphere-assisted imaging is highly fruitful in analyzing changes in the distribution pattern of proteins inside the

various cell types of a glomerulus. We are working on the optimization of microsphere-assisted super-resolution imaging technique further by controlling the imaging and microspheres properties that would allow us to study changes within the cell that can be induced through injury to the glomeruli.

5. CONCLUSION

In conclusion, we experimentally demonstrated the feasibility of performing super-resolution imaging of biological and photonic structures by using microspheres immersed in elastomers that allows production of novel microscope coverslips with super-resolution capability. Such microscope coverslips can be used with conventional microscopes to enhance the spatial resolution without the need for additional equipment. We investigated a potential application of our imaging technique for the observation of changes in the distribution pattern of proteins inside the various cell types of glomeruli cells in kidney tissues. Microsphere-assisted imaging technique is a promising candidate for applications in medical and cancer researches as well as in microfluidics and nanophotonics.

REFERENCES

[1] Darafsheh, A., [Optical super-resolution and periodical focusing effects by dielectric microspheres] Ph.D. dissertation, University of North Carolina at Charlotte, (2013).

[2] Darafsheh, A., Guardiola, C., Palovcak, A., Finlay, J. C., and Carabe, A., "Optical super-resolution imaging by high-index microspheres embedded in elastomers," Optics Letters 40(1), 5-8 (2015).

[3] Darafsheh, A., Limberopoulos, N. I., Derov, J. S., Walker, D. E., and Astratov, V. N., "Advantages of microsphere-assisted super-resolution imaging technique over solid immersion lens and confocal microscopies," Applied Physics Letters 104(6), 061117 (2014).

[4] Darafsheh, A., Walsh, G. F., Dal Negro, L., and Astratov, V. N., "Optical super-resolution by high-index liquid-immersed microspheres," Applied Physics Letters 101(14), 141128 (2012).

[5] Wang, Z., Guo, W., Li, L., Luk'yanchuk, B., Khan, A., Liu, Z., Chen, Z., and Hong, M., "Optical virtual imaging at 50 nm lateral resolution with a white-light nanoscope," Nature Communications 2, 218(6 pp) (2011).

[6] Heifetz, A., Kong, S.-C., Sahakian, A. V., Taflove, A., and Backman, V., "Photonic nanojets," Journal of Computational and Theoretical Nanoscience 6(9), 1979-1992 (2009).

[7] Darafsheh, A., and Astratov, V. N., "Periodically focused modes in chains of dielectric spheres," Applied Physics Letters 100(6), 61123 (2012).

[8] Darafsheh, A., Mojaverian, N., Limberopoulos, N. I., Allen, K. W., Lupu, A., and Astratov, V. N., "Formation of polarized beams in chains of dielectric spheres and cylinders," Optics Letters 38(20), 4208-4211 (2013).

[9] Darafsheh, A., Fardad, A., Fried, N. M., Antoszyk, A. N., Ying, H. S., and Astratov, V. N., "Contact focusing multimodal microprobes for ultraprecise laser tissue surgery," Optics Express 19(4), 3440-3448 (2011).

[10] Hutchens, T. C., Darafsheh, A., Fardad, A., Antoszyk, A. N., Ying, H. S., and Astratov, V. N., "Characterization of novel microsphere chain fiber optic tips for potential use in ophthalmic laser surgery," Journal of Biomedical Optics 17(6), 068004 (2012).

[11] Darafsheh, A., Hutchens, T. C., Fardad, A., Antoszyk, A. N., Ying, H. S., Fried, N. M., and Astratov, V. N., "Contact focusing multimodal probes for potential use in ophthalmic surgery with the Erbium:YAG laser," Proceedings of SPIE 8567, 856729 (2013).

[12] Hutchens, T. C., Darafsheh, A., Fardad, A., Antoszyk, A. N., Ying, H. S., Astratov, V. N., and Fried, N. M., "Detachable microsphere scalpel tips for potential use in ophthalmic surgery with the erbium:YAG laser," Journal of Biomedical Optics 19(1), 18003 (2014).

[13] Rayleigh, L., "Investigations in optics, with special reference to the spectroscope," Philosophical Magazine 8(49), 261-274 (1879).

[14] Houston, W. V., "A compound interferometer for fine structure work," Physical Review 29(3), 478-484 (1927).

[15] Goodman, J. W., [Introduction to Fourier Optics] Roberts and Company Publishers, Greenwood(2005).

[16] den Dekker, A. J., and van den Bos, A., "Resolution: a survey," Journal of the Optical Society of America A 14(3), 547-557 (1997).
[17] Menn-Josephy, H., and Beck, L. H. J., "Recurrent glomerular disease in the kidney allograft," Frontiers in Bioscience (Elite Ed.) 7, 155-170 (2015).